Available online at www.sciencedirect.com
SCIENCE DIRECT®
Journal of Solid State Chemistry 178 (2005) 1104–1111
JOURNAL OF SOLID STATE CHEMISTRY
www.elsevier.com/locate/jssc

Influence of *A*-site cation size on structural and physical properties in $Ca_{1-x}Sr_xMn_{0.96}Mo_{0.04}O_3$: A comparison of the $x = 0.3$ and 0.6 compounds

M. Miclau, S. Hébert*, R. Retoux, C. Martin

Laboratoire CRISMAT, UMR 6508 associée au CNRS, ENSICaen, 6 Boulevard du Maréchal Juin, 14050 Caen, Cedex, France

Received 11 October 2004; received in revised form 14 January 2005; accepted 16 January 2005

Abstract

Investigation of the electron-doped series $Ca_{1-x}Sr_xMn_{0.96}Mo_{0.04}O_3$ is reported. The magnetic, transport and structural properties have been characterized combining different techniques: X-ray diffraction, electron microscopy, magnetization, resistivity and thermopower measurements. For a constant small content of Mn^{+3} induced in the Mn^{+4} matrix by the Mo for Mn substitution, three crystallographic structures are evidenced, at room temperature, depending on the *A*-site size and the size mismatch effects. The influence of the structures on the transport and magnetic properties of these electron-doped manganites is presented. The optimization of the magnetoresistance and thermoelectric properties through the bandwidth parameter is presented.

Keywords: Perovskite; Manganite; Transport; Magnetic properties

1. Introduction

The numerous studies performed these last years about manganites with the perovskite structure have shown the extraordinary richness of the behaviors of these materials. Considering the general formula, $Ln_{1-x}A_xMnO_3$ where *Ln* is a trivalent lanthanide and *A* a divalent alkaline earth, two kinds of compounds can be mainly distinguished depending on *x*. The hole-doped manganites exhibit colossal magnetoresistance (CMR) for a rather wide composition range around $x \cong 0.3$ and require a large *A*-site cation size [1,2]. In contrast, the electron-doped manganites show CMR properties in a narrow range of composition around $x \cong 0.15$ and only for rather small *A*-site cations [3–6]. Despite the small CMR ratios observed in this electron-doped part of the phase diagram, compared to the hole-doped areas, this system is of great interest, particularly for the Ca-based manganites, by giving the opportunity to test models (canting or phase separation) proposed to explain the physical properties of manganites [7,8]. In fact, the low-temperature magnetic state of these compounds is complex, with the coexistence of ferromagnetism (FM) and C and G type of antiferromagnetism (AFM) whose amounts depend on *x* (in the range 0.8–1.0) [9,10]. Another way to introduce electrons, at such a low concentration in the Mn^{4+} matrix of $CaMnO_3$, consists in substituting manganese by cations with valence higher than 4+ [11]. The oxidation states of *B*-site cations have been determined by using thermopower measurements [12,13]. Among these series, the substitution by molybdenum leads to particularly interesting results due to its high valence state (+6) and its d^0 electronic configuration. A small content of Mo for Mn induces a large variation in the Mn valence (in accordance with the formula $Mo + 6xMn + 32xMn + 41 - 3x$), and only a slight distribution of the Mn lattice. A new structural and magnetic phase diagram is in this manner developed with interesting consequences for thermoelectric power properties [11–15].

*Corresponding author. Fax: +33 02 31 95 16 00.
E-mail address: sylvie.hebert@ensicaen.fr (S. Hébert).

0022-4596/$ - see front matter © 2005 Elsevier Inc. All rights reserved.
doi:10.1016/j.jssc.2005.01.025

A good thermoelement has to combine a large Seebeck coefficient together with a small resistivity to obtain a large power factor $PF = S^2/\rho$. The thermoelectric properties of $CaMn_{0.96}Mo_{0.04}O_3$ have been previously reported [14]. The small doping level is responsible for a metallic behavior together with a relatively large Seebeck coefficient at room temperature (RT), $S \sim -100\,\mu V/K$, which makes this material interesting as an *n*-type thermoelement. For a constant doping level, changing the *A*-site size was found to have a dramatic effect on the resistivity: in $SrMn_{0.96}Mo_{0.04}O_3$, the complete Sr for Ca substitution has induced a semiconducting like behavior, with still small values of ρ at RT, $\rho \sim 10^{-2}\,\Omega\,cm$ [12]. Moreover, as the Seebeck coefficient remains large and ρ small, this compound is also interesting for thermoelectricity. To understand the evolution from metallicity to semi-conducting behavior as a function of the *A*-site size, and try to find an optimum for thermoelements, we have investigated the whole series $Ca_{1-x}Sr_xMn_{0.96}Mo_{0.04}O_3$ with x ranging from 0 to 1. Moreover, the investigation of the $(Sr,Ca)MnO_3$ series has previously revealed attractive relationships between structural, transport and magnetic parameters [16]. We investigate here how a small electron content can affect these results, emphasizing the relationship between structure, magnetic properties, thermopower and magnetoresistance.

2. Experimental

The $Ca_{1-x}Sr_xMn_{0.96}Mo_{0.04}O_3$ samples with $0 \leqslant x \leqslant 1$ (by 0.1 step) have been prepared by mixing CaO, $SrCO_3$, MnO_2 and MoO_3 in stoichiometric proportions. The powders were first heated at 1000 °C with intermediate grindings and then pressed in the form of bars. They were then sintered first at 1200 °C for 12 h in air, and then at 1400 °C for 12 h—in air for $0 \leqslant x \leqslant 0.8$ and in argon for $x = 0.9$ and 1.0—slowly cooled to 800 °C and finally quenched to RT. Because the chemical titration for $x = 0.7$, 0.8, 0.9 and 1 showed a deficit in the oxygen content, these samples were annealed at 600 °C in oxygen flow, for 12 h. After the annealing, all the samples are oxygen stoichiometric.

The samples were first characterized at RT by X-ray diffraction. The patterns were obtained using a Philips diffractometer using Cu$K\alpha$ radiation, in the range $10 < 2\theta < 100°$, and the data were refined with the Fullprof program [17], showing the single phase nature of the samples. The electron diffraction (ED) and electron microscopy observations were also first performed at RT on JEOL 2010 and JEOL 2010F electron microscopes (tilt $\pm 60$and $\pm 42°$, respectively) equipped with Energy Dispersive Spectrometer (EDS) analyzers. EDS analyses of the different samples show that for these $(Ca,Sr)(Mo,Mn)O_3$ manganites, the cationic compositions of the crystallites are identical to the nominal ones in the limit of the errors. The reciprocal lattice reconstruction performed on several crystals of each preparation allowed us to confirm, depending on the x values, the *Pnma* and $I4/mcm$ space groups determined by X-ray diffraction at RT.

A few measurements were also done vs. temperature, by X-ray diffraction—from 100 to 400 K—and by electron microscopy. For the latter study, double tilt liquid nitrogen cooled sample holders were used in the range 100–300 K.

Resistivity ($5\,K \leqslant T \leqslant 400\,K$), TEP and thermal conductivity ($5\,K \leqslant T \leqslant 320\,K$) were all measured in the same Physical Properties Measurements System (Quantum Design), that also allows magnetic field scans in the range 0–9 T. The resistance was measured with the four-probe technique on $2 \times 2 \times 10$ mm bars. For the thermopower measurements, the four points steady-state method, with separated measuring and power contacts, was used to eliminate the thermal resistance between the sink and the heater, respectively.

Magnetization data were collected with a SQUID magnetometer (5–400 K, 0–5 T).

3. Results and discussion

3.1. Structural analysis

The study of the X-ray patterns of $Ca_{1-x}Sr_xMn_{0.96}Mo_{0.04}O_3$ recorded at RT shows a transition from the *Pnma* space group ($a_p\sqrt{2}$, $2a_p$, $a_p\sqrt{2}$) for $x \leqslant 0.5$ to $I4/mcm$ ($a_p\sqrt{2}$, $2a_p$) for $0.5 < x \leqslant 0.7$. For the higher x values ($x > 0.7$), the structure becomes cubic ($Pm3m$), a_p referring to the cell parameter of the ideal cubic perovskite (≈ 3.8 Å). Even if the cell volume increases regularly with x (not shown), in agreement with the larger size of Sr compared to Ca (1.31 and 1.18 Å, respectively) [18], the description of the evolution of the cell parameters is more difficult due to the existence of the different space groups. Such *Pnma* to $I4/mcm$ and further to $Pm3m$ transitions are commonly observed in perovskite manganites and are attributed to the average *A*-site size ($\langle r_A \rangle$) effect. In fact, this structural evolution vs. $\langle r_A \rangle$, at fixed Mn valence (here +3.92, due to the +6 oxidation state of Mo) can be compared to those reported for $Sr_{1-x}Ca_xMnO_3$ [16] (with +4 as Mn valence), for which the size and mismatch [19] effects have been reported and compared with the $Sr_{1-y}Ba_yMnO_3$ series.

In order to illustrate the structural aspect of this series, two compositions—belonging to *Pnma* and $I4/mcm$ space groups—have been selected for a more detailed study. The $x = 0.3$ compound is characteristic of the *Pnma* area, as shown by the RT X-ray and [010] ED patterns given in Fig. 1. It exhibits a pseudo-cubic

cell with close a, $b/\sqrt{2}$ and c parameters [$a = 5.3338(2)$, $b = 7.5343(4)$, $c = 5.3249(2)$ Å]. This structure is characterized by regular MnO_6 octahedra with two shorter and two longer Mn–O distances in the basal plane (≈ 1.88 and 1.92 Å) and two intermediate apical distances of ≈ 1.91 Å. An orthorhombic to monoclinic transition has been evidenced when the temperature is lowered down to 100 K (Fig. 2). The splitting of the spots involved by the monoclinic distortion of the cell is clearly evidenced in the [010] ED pattern if an enlargement of that diffraction pattern is performed (presented Fig. 2b). Here the splitting of the spots shows the angle of the monoclinic distortion. This very small angle ($\varepsilon < 1°$) is symbolized by two white lines forming a 2ε angle. Associated to the splitting of the diffraction spots, the appearance of parallel domains correlated to the coexistence of homogeneous monoclinic areas in the grains is clearly visible in dark field images as shown in Fig. 2c. The small deviation involved by the monoclinic distortion induces few strains in the grains and the appearance of these quite large parallel domains can be directly linked to the reduction of these strains in the grains. A larger ε angle should have created smaller domains to reduce the induced strains. The transition temperature between the monoclinic and orthorhombic structures deduced from these observations is close to 115 K and can be compared to the transition temperature deduced from the magnetic measurements. This slight monoclinic distortion is not very visible in the 100 K X-ray diffraction pattern (not shown) with a β angle refined to $\approx 90.5°$. This temperature dependence of the structure is in contrast to the observations performed on the pure calcium parent compound $CaMn_{0.96}Mo_{0.04}O_3$ which remains *Pnma* whatever the temperature (from 90 to 300 K). But this behavior is similar to the one reported for $CaMn_{0.9}Mo_{0.1}O_3$ [13].

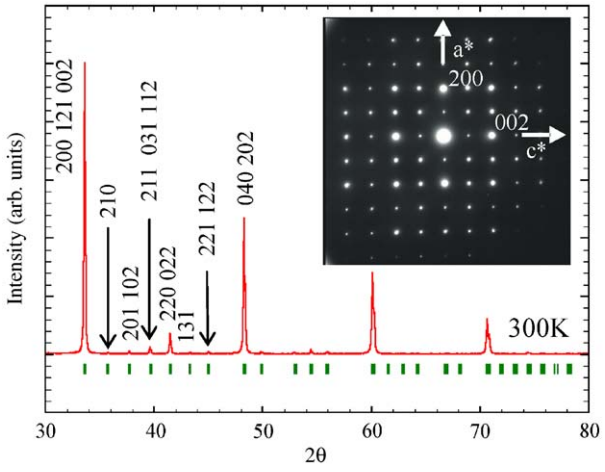

Fig. 1. RT X-ray pattern of the $x = 0.3$ compound, the *Pnma* Bragg positions are given, and the corresponding [010] ED pattern is inset.

The RT cell parameters of the $x = 0.6$ sample, belonging to the $I4/mcm$ zone as shown by the X-ray and [001] ED patterns given Fig. 3, are refined to $a = 5.3417(1)$ and $c = 7.6355(2)$ Å. As for the $x = 0.3$ manganite, it corresponds to regular (slightly elongated) MnO_6 octahedra with four equatorial Mn–O distances of ≈ 1.895 Å, the two apical being ≈ 1.91 Å. In that case, by decreasing the temperature, no monoclinic distortion is observed by electron microscopy. But, increasing the temperature, the tetragonal distortion decreases progressively from 100 to 400 K, as shown by the X-ray diffraction patterns in inset of Fig. 3. Probably the structure becomes cubic at higher temperatures, and it is clear that the transition is very smooth. It is in agreement with the broad bump observed around 320 K in the $M(T)$ curve (see Fig. 4 in the following).

To summarize this short structural section:

- At RT, the space group evolves for *Pnma* to $I4/mcm$ and then $Pm3m$ in agreement with the increase of $\langle A \rangle$ site cationic size.
- Nevertheless, the MnO_6 octahedra remain regular at RT, in accordance with the high Mn valence (+3.92).
- The temperature dependence of the structures shows various transitions—depending on the Ca/Sr ratio—leading to a complex phase diagram.

3.2. Magnetic properties

The influence of the Sr for Ca substitution on the magnetic properties is summarized in Fig. 4. The $M(T)$

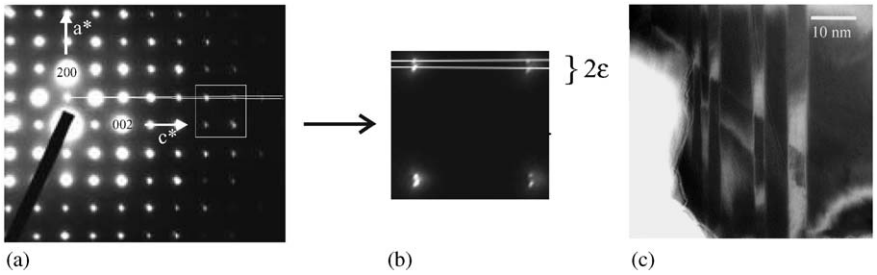

Fig. 2. $x = 0.3$ compound 100 K [010] ED pattern enlargement of (a), the white lines drawn on the pattern show the very small ε angle of the monoclinic distortion ($\varepsilon \approx 0.5°$). Dark field image recorded along the [010] zone axis at 100 K, large parallel domains (several nanometers wide), due to the slight monoclinic distortion, are clearly visible.

curves of three characteristic samples $x = 0$, 0.3 and 0.6, recorded in 0.3 T after zero field cooling and field cooling, are shown. As the Sr content increases, the magnetization decreases in the whole T range. All the curves show two distinct transitions for $x \neq 0$. The first one is observed at low T, ~100 K, while the second one (marked by the arrow) corresponds to the maximum of magnetization observed at high T. This high T maximum, usually associated with orbital ordering (OO), strongly increases from ~125 to ~320 K as the Sr content increases from 0.3 to 0.6. In the following, this transition temperature will be referred to T_{OO}.

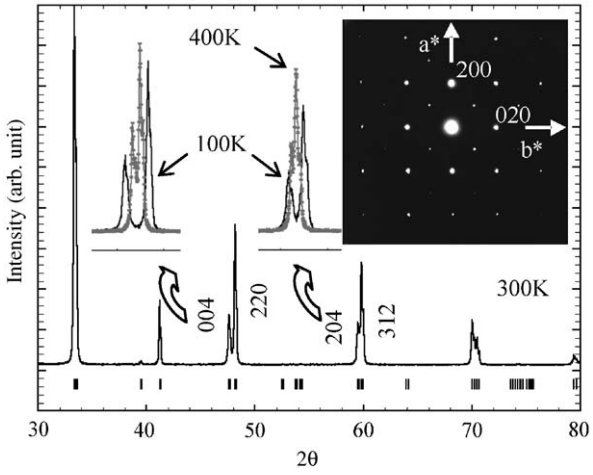

Fig. 3. RT X-ray and [001] ED patterns of $Ca_{0.4}Sr_{0.6}Mn_{0.96}Mo_{0.04}O_3$. The Bragg positions correspond to the $I4/mcm$ space group. The selected parts of the 100 and 400 K patterns show the decrease of the tetragonal distortion with the increase of the temperature.

The $\chi^{-1}(T)$ curves exhibit a Curie–Weiss behavior at high T (inset of Fig. 4). The θ_p extracted values decrease as x increases, changing from +30 K for $x = 0.3$ to −130 K for $x = 0.6$. This evolution reflects the strengthening of the AFM character in these compounds as the Sr content increases. The values of μ_{eff} extracted from these curves are in the range 3.74–3.96 μ_B/f.u., which is consistent with the theoretical expectation of 3.88 μ_B/f.u. for $Ca_{1-x}Sr_xMn^{3+}_{0.08}Mn^{4+}_{0.88}Mo^{6+}_{0.04}O_3$.

The Sr for Ca substitution has thus two effects on the magnetic properties: the magnetization decreases in the whole T range and there appears a maximum of $M(T)$ at high temperature, linked to the structural transitions, as discussed previously for $x = 0.3$ and 0.6. Without electron doping (i.e., without Mo), the Sr for Ca substitution induces also a decrease of the magnetization [16]. But on the other hand, no high-temperature clear maximum was observed on the $M(T)$ curves in $Ca_{1-x}Sr_xMnO_3$ [16], i.e., for compounds with only Mn^{4+}. The electron doping, induced by Mo, is thus responsible for this high-temperature $M(T)$ maximum. For comparison, in the $CaMn_{1-x}Mo_xO_3$ series [13], it was found that by electron doping, OO can be induced starting from x~0.06, i.e., for a Mn valency close to 3.87. Neutron diffraction and high-resolution electron microscopy studies [13,15] have investigated the relationship between the e_g OO and the Mn^{3+} content. In the present study, by tuning the structural parameters via the $\langle r_A \rangle$ size (i.e., via the Sr content), the concentration of electrons required to get OO becomes smaller than in the $CaMn_{1-x}Mo_xO_3$ compounds: the Mn valency is close to +3.92. Orbital and charge

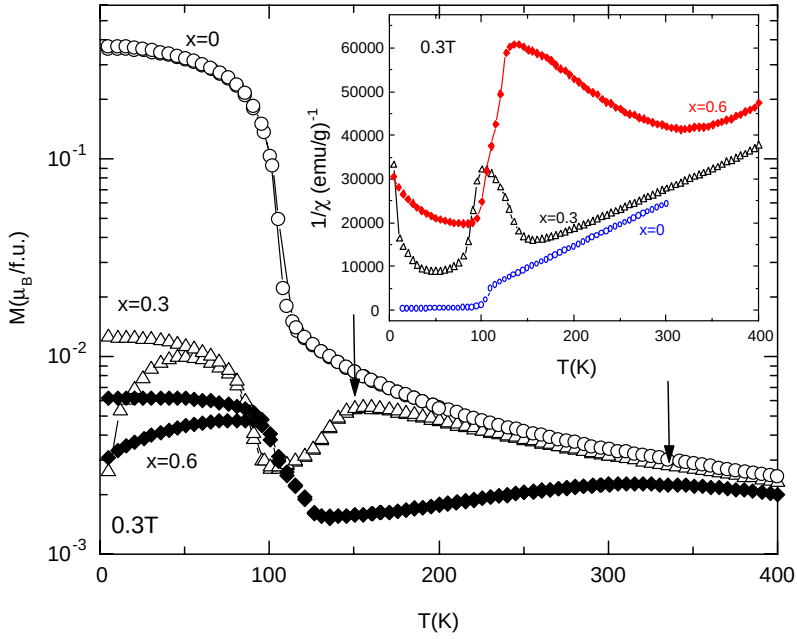

Fig. 4. Temperature dependences of zero field cooled and field cooled magnetization under 0.3 T for $Ca_{1-x}Sr_xMn_{0.96}Mo_{0.04}O_3$. Inset: inverse of susceptibility vs. temperature for the same compounds.

ordering have already been observed in compounds with a very small concentration of e_g electrons, e.g., as in $Ca_{1-x}Ce_xMnO_3$ [20,21], where these phenomena are observed for an Mn valency of 3.85. This shows that CO/OO can be observed even in the presence of a very low concentration of e_g electrons, depending on the *A*-site size. The common result between these different systems is that T_{OO} is very high, close to 320 K. It is significantly higher than those observed in (*Ln*,Ca)M-nO$_3$ systems [4,21] but it is close to those reported for the (Pr,Sr)MnO_3 series [22]. The origin of such a high T_{OO} is still unclear.

3.3. Transport properties

The resistivity curves of these samples are presented in Fig. 5. The growth of AFM interactions is associated to a strong increase of the resistivity at low *T*, increasing from $10^{-2}\,\Omega$cm for $x=0$ to $5\times10^{5}\,\Omega$cm for $x=0.6$ at 5 K. For the low Sr content, a metallic behavior is observed at high *T* (above 200 K for $x=0$ and 280 K for $x=0.3$). The metallicity is shifted to higher temperature as the Sr content increases and for $x>0.4$, the materials present a semi-conducting-like behavior ($d\rho/dT<0$) in the whole range of temperature investigated here, from 5 to 400 K. Moreover, for $x\geqslant0.3$, there is a spectacular increase of the $\rho(T)$ curves at *T* close to T_{OO} (Fig. 5). This sharp increase of ρ is usually associated to an OO transition, e.g., as in $CaMn_{1-x}Mo_xO_3$ [13].

The effect of a magnetic field is shown in Fig. 6. The magnetoresistance $\rho(0\,T)/\rho(7\,T)$ goes through a large maximum of 300 (corresponding to a MR ratio $MR(\%)=100(\rho(7\,T)-\rho(0\,T))/\rho(0\,T)$ of –100%) at 5 K for $x=0.15$ then decreases and reaches 1 for $x=0.3$. The scenario for this MR at low *T* is the following. For $CaMnO_3$, FM interactions coexist with AFM [23,24] and the Mo for Mn substitution induces a mixture of Mn^{3+}/Mn^{4+} favoring the double-exchange

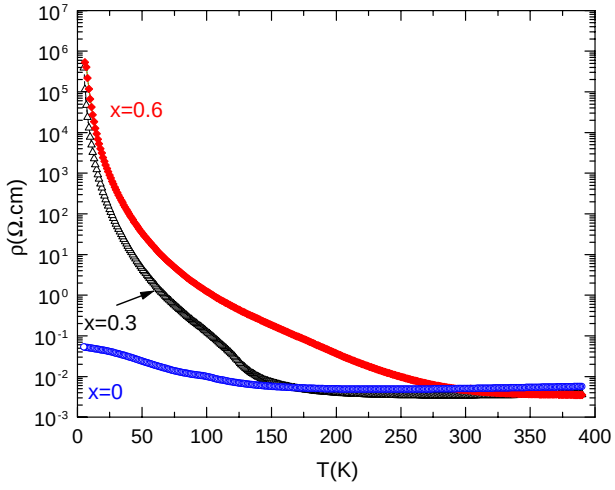

Fig. 5. Resistivity curves of $Ca_{1-x}Sr_xMn_{0.96}Mo_{0.04}O_3$ under 0 T.

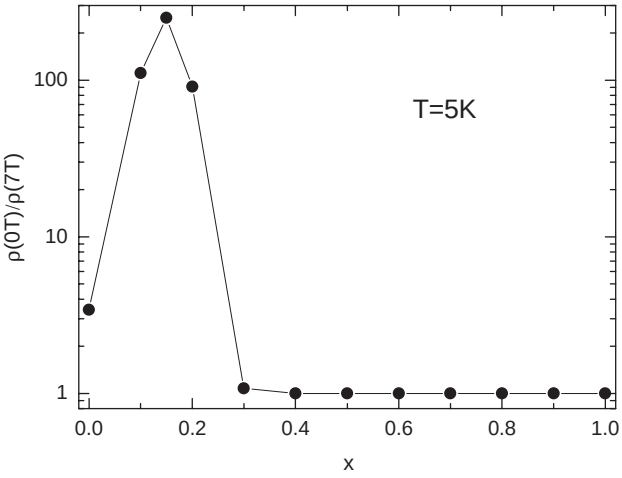

Fig. 6. CMR effect at 5 K: $[\rho(0\,T)/\rho(7\,T)]$ vs. *x*.

interactions and thus magnetoresistance. As the Sr content slightly increases, the FM fraction decreases as shown on the $M(T)$ curves (Fig. 4) but remains strong enough to induce MR at low *T*. The maximum of MR corresponds thus to the sample combining a high resistivity together with a large enough magnetization ($x=0.15$). For $x>0.3$, the maximum of magnetization at T_{OO} is more pronounced, and *M* at low *T* is reduced by a factor of 10 compared to $x=0$. In these strongly AFM samples, the FM fraction, if it exists, is too small to induce any MR. The only effect of the magnetic transition on the $\rho(T)$ curves is a small inflexion.

As shown previously in other manganites, the thermopower measurements *S* are very sensitive to the magnetic and structural transitions [25]. Fig. 7 presents the $S(T)$ curves for $x=0$, 0.3, and 0.6. First we will focus on the high-temperature data for $x=0$ and 0.3. At high temperature, the curves are almost superimposed, with $S_{300K}\sim-110\,\mu V/K$ and varying linearly with *T* for $x=0$ and 0.3. From the slopes of $S(T)$ at high *T*, using

$$S=\frac{\pi^2k_B^2T}{3e}\left[\frac{\partial\ln n(E)}{\partial E}+\text{cste}\right]\Bigg|_{E=E_F},$$

where $n(E)$ is the carrier density, and a width of conduction band of ~1 eV [26], the ratio $N(E)/n=11$, with $N(E)$ the density of states, in good agreement with the theoretical value of $n(Mn)/n(Mn^{3+})=12$ for these $Ca_{1-x}Sr_xMn^{3+}_{0.08}Mn^{4+}_{0.88}Mo^{6+}_{0.04}O_3$ samples. The slopes for $x=0$ and 0.3 are similar, reflecting the constant doping level.

For $x=0$, as *T* decreases, *S* remains negative as expected for electron doping, and decreases down to 0, with a small accident observed at $T_N\sim110$ K. For $x=0.3$, *S* is negative in the whole *T* range. At low *T*, its magnitude is larger than for $x=0$, which correlates with the more insulating behavior observed for $x=0.3$ than for $x=0$ below 150 K. Two transitions are observed on

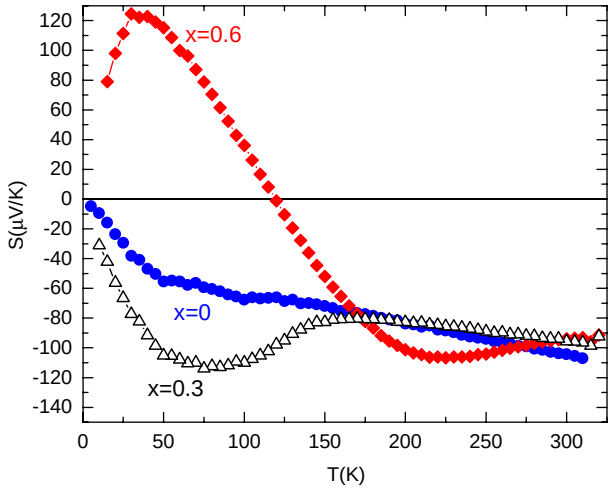

Fig. 7. T-dependent thermopower of $Ca_{1-x}Sr_xMn_{0.96}Mo_{0.04}O_3$ (for $x = 0$, 0.3, 0.6).

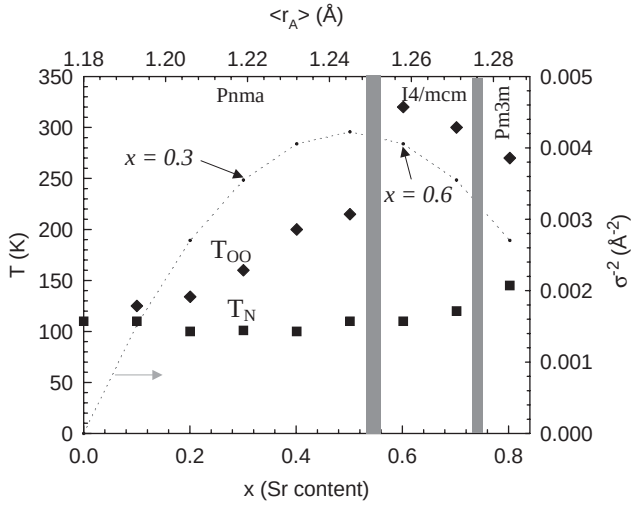

Fig. 8. (T,x) phase diagram of $Ca_{1-x}Sr_xMn_{0.96}Mo_{0.04}O_3$. The characteristic temperatures are extracted from the $M(T)$ curves. The x (top) and y (right)-axis are also given in $\langle r_A \rangle$ and σ^2, respectively, to show the influence of the mismatch on the characteristic temperatures. The gray areas are only for the boundaries between the three space groups which are not determined with accuracy (due to the step of 0.1 in the compositions).

the $S(T)$, the first one at ~150 K with a strong increase of $|S|$, usually observed in the case of OO [27], and the second one at ~100 K corresponding to T_N.

For $x = 0.6$, the high-T linear regime, if it exists, is not reached. In this material, T_{OO}~320 K and our data are restricted to $T \leqslant 320$ K. However, the value at 320K is similar to the one of $x = 0$ and 0.3. This can be crudely explained considering the Heikes formula [28], which states that at very high T, the limit of S only depends on the carrier concentration. Below 320 K, a strong inflection and increase of $|S|$ are observed, typical of OO as for $x = 0.3$. Then below 200 K, $|S|$ decreases again, reaches 0 and becomes positive, up to $+120\,\mu V/K$ at 50 K. Even if the materials are electron doped, this positive thermopower at low T is observed in all the Sr-rich compounds and the temperature at which S crosses 0 evolves from 50 K for $x = 0.5$ (not shown here) to 125 K for $0.6 \leqslant x \leqslant 1$.

Such a change of sign of S as a function of the A-site size was observed previously in the $Pr_{0.7}Ca_{0.3-x}Sr_xMnO_3$ compounds, for which the doping level is constant with a fixed $Mn^{3.3+}$ valence, i.e., for hole-doped oxides [25]. In this case, the effect is opposite, S at high temperature going from positive for Ca-rich compounds to negative for Sr-rich compounds. To understand this evolution, the importance of the band structure on the sign of S was emphasized. In the electron-doped $CaMn_{1-x}Mo_xO_3$ series, such a change of sign was also observed as a function of x, and this was linked to a structural transition [13]. In these compounds, the change of sign appears at low T, in the magnetic state, and is very similar to what is observed here in $Ca_{1-x}Sr_xMn^{3+}_{0.08}Mn^{4+}_{0.88}Mo^{6+}_{0.04}O_3$. For $CaMn_{1-x}Mo_xO_3$, the positive Seebeck coefficient was attributed to the higher electron density in $3d_{z^2-r^2}$ orbitals due to the elongation of the MnO_6 octahedra, resulting in hole-like carriers hopping in the ferromagnetic chains of this C-type antiferromagnet. Our results, in the $Ca_{1-x}Sr_xMn_{0.96}Mo_{0.04}O_3$ series, show that indeed, for a constant doping level of electrons, the Seebeck coefficient can be positive, depending on the structural distortion. Here the change of sign of S is observed first for $x = 0.5$, i.e., for the maximum mismatch value σ^2 (Fig. 8). This parameter represents the disorder induced by the random distribution of cations with different size in the same crystallographic site (here Ca and Sr) [19]. This maximum also corresponds to the orthorhombic to tetragonal transition. The magnetic structure of the $x \geqslant 0.5$ samples is not known yet, but we can infer that a similar mechanism as in $CaMn_{1-x}Mo_xO_3$ might be at the origin of the positive S value. Structural and magnetic studies, vs. temperature, by neutron diffraction would be necessary to confirm this hypothesis.

Concerning the thermoelectric performances of these materials, a slight increase of the Power Factor at RT is obtained for $x = 0.6$ ($2.6 \times 10^{-4}\,WK^{-2}m^{-1}$ for $x = 0.6$ compared to $1.1 \times 10^{-4}\,WK^{-2}m^{-1}$ for $x = 0$, and 3.6×10^{-5} for $x = 1$ [12]). The most important result is not this value by itself, but the temperature dependence of PF. In these compounds, S increases linearly with T up to 800 K [29], and a similar behavior should be observed for $x = 0.6$. Moreover, the semi-conducting-like behavior of $x = 0.6$ will induce an increase of PF as T increases. This makes this compound very promising for high-temperature applications.

4. Conclusion

The structural study performed here is not sufficient to draw a detailed structural and magnetic $\langle T,x \rangle$ phase

diagram. Nevertheless, the preliminary RT structural results show the same trend as in the $Sr_{1-x}Ca_xMnO_3$ series [16,30,31]. In both series, as $\langle r_A \rangle$ increases, the space group changes from *Pnma* to $I4/mcm$ and then to $Pm3m$, in agreement with the increase of $\langle r_A \rangle$. Nevertheless, in the title series, a new structure—compared to $Sr_{1-x}Ca_xMnO_3$ [16]—has been evidenced with a monoclinic distortion at low temperature for $x = 0.3$.

The size mismatch appears, for both series [16 and this work], as a relevant parameter to explain the evolution of the transition temperatures which first increase and then decrease when $\langle r_A \rangle$ increases continuously. This is illustrated by the $T_{OO}(x)$ dependence, reported in Fig. 8, the optimum of T_{OO} corresponds roughly to the maximum of σ^2. This $\langle T,x \rangle$ phase diagram, established from magnetization measurements, also shows that, in contrast, the magnetic transition temperature T_N remains nearly constant, even if the FM component decreases with x (Fig. 4). In fact, as in $Sr_{1-x}Ca_xMnO_3$, the AFM interactions increase with the Sr content. But in the series under study, due to the electron doping, the OO is reinforced.

A neutron diffraction study is planned (i) to determine the magnetic transition temperatures of several compounds, to know if—as T_{OO}—they follow the same x dependence (similarly to the evolution of T_N in $Sr_{1-x}Ca_xMnO_3$) and (ii) to try to correlate the structural distortions (vs. T) and the observed variation of thermopower sign. This study is necessary to know accurately the oxygen positions (and thus the MnO_6 distortions) to understand why similar physical properties (a bump of $M(T)$ and an increase of $\rho(T)$ at T_{OO}) are observed for compounds with different space groups.

It has been shown in previous reports [5,6,9,10] that the Mn^{+4}-rich compounds reveal various unusual behaviors, in connection with mesoscopic magnetic and crystallographic phase separation. In this framework, this electron-doped system (Ca,Sr)(Mn,Mo)O_3 is really very interesting because, due to its high oxidation state (+6) and its d^0 electronic configuration, small Mo contents induce large amounts of Mn^{+3}, without disturbing the Mn lattice. It is why magnetic and/or OO can develop at high temperatures (depending on the electron doping). Then, playing on the Sr for Ca substitution, it is possible to fit the geometrical parameters to control the properties, via the FM/AFM ratio. In particular, charge ordering can be found in this series for a very small content of e_g electrons, in the case of large r_A size. In this way, an optimal CMR ratio (≈ 300) is obtained for $Ca_{0.85}Sr_{0.15}Mn_{0.96}Mo_{0.04}O_3$. Also, the Power Factor at RT has been found to be the largest for $x = 0.6$, and will be maximized at higher temperature. Due to the good chemical stability of these compounds at high temperature, this material could be used for *n*-type thermoelements at high T ($T > 300$ K).

Acknowledgments

The authors would like to thank Maryvonne Hervieu and Antoine Maignan (Laboratoire CRISMAT) for their constructive remarks.

This work was supported by the European Union, under contract No. HPMT_CT_2000_00141 (MM).

References

[1] C.N.R. Rao, B. Raveau (Eds.), Colossal Magnetoresistance, Charge Ordering and Related Properties of Manganese Oxides, World Scientific, Singapore, 1998.
[2] Y. Tokura (Ed.), Colossal Magnetoresistive Oxides, Gordon and Breach Science Publishers, New York, 1999.
[3] A. Maignan, C. Martin, F. Damay, B. Raveau, Chem. Mater. 10 (1998) 950.
[4] C. Martin, A. Maignan, M. Hervieu, B. Raveau, Phys. Rev. B 60 (1999) 12191.
[5] C. Martin, A. Maignan, M. Hervieu, B. Raveau, Z. Jirak, A. Kurbakov, V. Trounov, G. André, F. Bourée, J. Magn. Magn. Mater. 205 (1999) 184.
[6] C. Martin, A. Maignan, M. Hervieu, B. Raveau, Z. Jirak, M.M. Savosta, A. Kurbakov, V. Trounov, G. André, F. Bourée, Phys. Rev. B 62 (2000) 6442.
[7] P.G. de Gennes, Phys. Rev. 118 (1960) 141.
[8] A. Moreo, S. Yunoki, E. Dagotto, Science 283 (1999) 2034.
[9] C.D. Ling, E. Granado, J.P. Neumeier, J.W. Lynn, D.N. Argyriou, Phys. Rev. B 68 (2003) 144439.
[10] E. Granado, C.D. Ling, J.P. Neumeier, J.W. Lynn, D.N. Argyriou, Phys. Rev. B 68 (2003) 144440.
[11] B. Raveau, Y.M. Zhao, C. Martin, M. Hervieu, A. Maignan, J. Solid State Chem. 149 (2000) 203.
[12] A. Maignan, S. Hébert, L. Pi, D. Pelloquin, C. Martin, C. Michel, M. Hervieu, B. Raveau, Cryst. Eng. 5 (2002) 365.
[13] A. Maignan, C. Martin, C. Autret, M. Hervieu, B. Raveau, J. Hejtmanek, J. Mater. Chem. 12 (2002) 1806.
[14] L. Pi, S. Hébert, C. Martin, A. Maignan, B. Raveau, Phys. Rev. B 67 (2003) 024430.
[15] C. Martin, A. Maignan, M. Hervieu, B. Raveau, J. Hejtmanek, Phys. Rev. B 63 (2001) 100406(R).
[16] O. Chmaissem, B. Dabrowski, S. Kolesnik, J. Mais, D.E. Brown, R. Kruk, P. Prior, B. Pyles, J.D. Jorgensen, Phys. Rev. B 64 (2001) 134412.
[17] J. Rodriguez-Carvajal, Physica B 192 (1993) 55.
[18] R.D. Shannon, Acta Crystallogr. A 32 (1976) 751.
[19] L.M. Rodriguez-Martinez, J.P. Attfield, Phys. Rev. B 54 (1996) R15622.
[20] Z. Zeng, M. Greenblatt, M. Croft, Phys. Rev. B 63 (2001) 224410.
[21] E.N. Caspi, M. Avdeev, S. Short, J.D. Jorgensen, M.V. Lobanov, Z. Zeng, M. Greenblatt, P. Thiyagarajan, C.E. Botez, P.W. Stephens, Phys. Rev. B 69 (2004) 104402.
[22] P. Schiffer, A.P. Ramirez, W. Bao, S.W. Cheong, Phys. Rev. Lett. 75 (1995) 3336.
[23] J.B. MacChesnay, H.J. Williams, J.F. Potter, R.C. Sherwood, Phys. Rev. 164 (1967) 779.

[24] J.J. Neumeier, J.L. Cohn, Phys. Rev. B 61 (2000) 14319.
[25] J. Hejtmanek, Z. Jirak, D. Sedmidubsky, A. Maignan, Ch. Simon, V. Caignaert, C. Martin, B. Raveau, Phys. Rev. B 54 (1996) 11947.
[26] J. Hejtmanek, Z. Jirak, M. Marysko, C. Martin, A. Maignan, M. Hervieu, B. Raveau, Phys. Rev. B 60 (1999) 14057.
[27] J. Hejtmanek, Z. Jirak, Z. Arnold, M. Marysko, S. Krupicka, C. Martin, F. Damay, Appl. Phys. 83 (1998) 7204.
[28] R.R. Heikes, R.W. Ure, Thermoelectricity: Science and Engineering, Interscience Publishers, New York, London, 1961.
[29] S. Hébert, D. Flahaut, D. Pelloquin, C. Martin, A. Maignan, Proceedings of the 21st International Conference on Thermoelectricity, 2003.
[30] H. Taguchi, M. Sonoda, M. Nagao, J. Solid State Chem. 137 (1997) 82.
[31] J.S. Zhou, J.B. Goodenough, Phys. Rev. B 68 (2003) 054403.